Chapter VII

Myoelectric Teleoperation of a Dual-Arm Manipulator Using Neural Networks

Toshio Tsuji, Hiroshima University, Japan

Kouji Tsujimura, OMRON Corporation, Japan

Yoshiyuki Tanaka, Hiroshima University, Japan

Abstract

In this chapter, an advanced intelligent dual-arm manipulator system teleoperated by EMG signals and hand positions is described. This myoelectric teleoperation system employs a probabilistic neural network, so called log-linearized Gaussian mixture network (LLGMN), to gauge the operator's intended hand motion from EMG patterns measured during tasks. In addition, an event-driven task model using Petri net and a non-contact impedance control method are introduced to allow a human operator to maneuver a couple of robotic manipulators intuitively. A set of experimental results demonstrates the effectiveness of the developed prototype system.

Introduction

Many researchers have actively studied teleoperation technology as an effective human interface for supporting an operator in various tasks. However, current technology is still far from realizing an autonomous robotic system that has high intelligence for auto-recognition and judgment in human task situations. If the operator can control a tele-exist slave-robot as his own arm with natural feeling, task performance will increase.

In this chapter, an advanced intelligent dual-arm manipulator system teleoperated by EMG signals and hand positions is described. The presented myoelectric teleoperation system employs a probabilistic neural network, so called log-linearized Gaussian mixture network (LLGMN), to gauge the operator's intended hand motion from EMG patterns measured during tasks. In addition, an event-driven task model using Petri net and a non-contact impedance control method are introduced to allow a human operator to maneuver a couple of robotic manipulators intuitively. A set of experimental results demonstrates the effectiveness of the developed prototype system.

Background

In the late 1940s, Argonne National Laboratory developed the first teleoperation system that could handle radioactive materials in a nuclear reactor using a robotic manipulator from outside. The motion of the master-arm was transmitted to the slave-arm in the nuclear reactor via a mechanical link structure (Sheridan, 1992). Fundamental concept of current teleoperation systems using electric signals was proposed by Goertz (1954). Since then, many researchers have actively studied teleoperation technology as an effective human interface for supporting an operator in various tasks (Shimamoto, 1992; Yokokohji & Yoshikawa, 1994; Yoon et al., 2001; Mobasser et al., 2003; Ueda & Yoshikawa, 2004).

Some teleoperation tasks require dexterous manipulation of a robotic arm. If the operator can control a tele-exist slave-robot as his own arm with natural feeling, task performance will increase. However, controlling the robot manipulator by means of a conventional interface system, such as a joystick or a master-arm robot, is difficult because it requires highly skilled and experienced system operators. Experimental studies utilizing bioelectric signals, such as electroencephalogram (EEG) and electromyogram (EMG) as an input of the interface system have been undertaken (Farry et al., 1996; Kim et al., 2001; Englehart & Hudgins, 2003; Suryanarayanan & Reddy, 1997;Tsujiuchi et al., 2004; Wolpaw

et al., 1998). However, since previous studies focused mainly on reproducing the specified operator's motions by a robotic device, it is almost impossible to apply those proposed systems to practical situations in an actual task environment in which human-like skillful and flexible movements, as well as the cooperative operation of a dual arm, will be required.

This chapter argues cybernetic control of a dual-arm manipulator system teleoperated by EMG signals and hand positions, in which the operator can control two manipulators intuitively by his arm movements with regulating muscle contraction levels. To realize skillful cooperative operations of the dual arm in general task environments, the developed system employs an event-driven task model and a non-contact impedance control method. Moreover, high recognition performance is achieved by using a posterior neural network that can adapt the variation of the EMG signals caused by individual differences, electrode locations, physical fatigue, and perspiration.

An Intelligent EMG-Based Dual-Arm Manipulator System

Figure 1 illustrates the control structure of the proposed teleoperation system using EMG signals, where the system consists of the forearm control part and the upper arm control part for each arm. The prosthetic hand (Imasen lab.) is attached as each end-effector of two robotic manipulators (Move Master RM-501: Mitsubishi Electric Corp.), and each arm has seven DOFs as illustrated in Figure 2. In this system, the section from the first to third link is defined as the upper arm part, while the rest, including the end-effector, as the forearm part. The positive joint rotational direction and the standard link posture of the forearm are presented in Figure 2.

Forearm Control Part

The forearm control part processes the measured EMG signals transmitted by the wireless equipment and extracts feature patterns corresponding to the operator's intended motion. This subsection explains one arm of the dual-arm system. Each motion of the forearm's joints (J_{4w}, J_{5w}, J_{6w}, J_{7w}) is controlled according to the operator's intended motion, estimated by the trained neural network. System parameters are then regulated automatically so that dynamic properties of the robotic arm are adapted for the task model of a given task. In addition, the forearm motion uses impedance control to realize human-like skillful

Figure 1. The dual-arm manipulator system using EMG signals

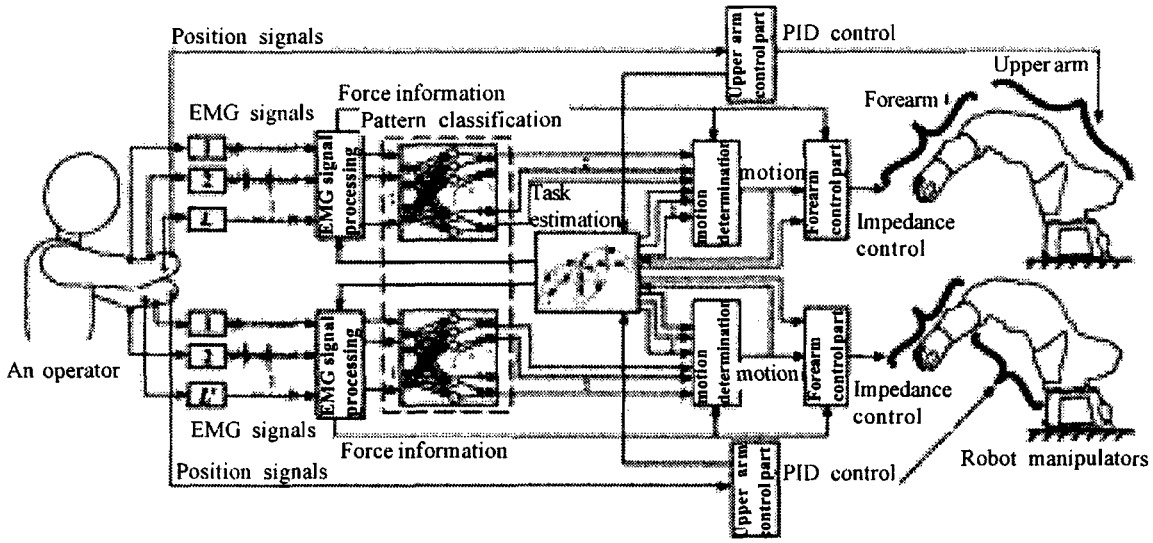

Figure 2. A link model of the robot manipulator

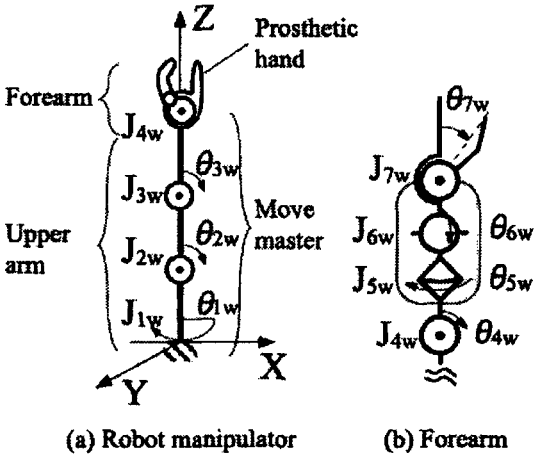

movements in the coordinated task by dual arms. Detailed explanations of each function in the control system are given below.

EMG Signal Processing

EMG signals measured from L pairs of electrodes attached at one arm of the operator are digitized by an analog-to-digital (A/D) converter (sampling frequency 1.0 [kHz]). Then, the digitized data are amplified, rectified, and filtered through a digital second-order Butterworth filter (cut-off frequency: 1.0 [Hz]). These sampled signals are defined as $EMG_l(n)$ ($l = 1,2,\cdots,L$).

EMG patterns are extracted from a set of $EMG_l(n)$ and represented as a feature pattern vector $\mathbf{x}(n) = [x_1(n), x_2(n), \cdots, x_L(n)]^{\mathrm{T}} \in \Re^L$ by

$$x_l(n) = \frac{EMG_l(n) - \overline{EMG_l}^{st}}{EMG_l^{max} - \overline{EMG_l}^{st}} \sum_{i=1}^{L} \frac{EMG_i^{max} - \overline{EMG_i}^{st}}{EMG_i(n) - \overline{EMG_i}^{st}}, \tag{1}$$

where $\overline{EMG_l}^{st}$ denotes the mean value of $EMG_l(n)$ measured in relaxing the muscles, and EMG_l^{max} are the values of EMG signals measured in the maximum voluntary contraction. Notice that $\mathbf{x}(n)$ is normalized to make its norm equal 1. Also, using EMG signals, the force information in arm movements is calculated by

$$F_{EMG}(n) = \frac{1}{L} \sum_{l=1}^{L} \frac{EMG_l(n) - \overline{EMG_l}^{st}}{EMG_l^{max} - \overline{EMG_l}^{st}}. \tag{2}$$

The value of $F_{EMG}(n)$ is utilized as a measurement to decide whether the operator takes an action for operating the robotic arm or not.

Pattern Classification Using Probabilistic Neural Networks

An extracted EMG pattern is regarded as a stochastic one since the EMG signal is the composition of spike potentials generated in the muscle fibers. In this study, a log-linearized Gaussian mixture network (LLGMN) (Tsuji et al., 1994, 1999; Fukuda et al., 2003) is utilized as a neural network to estimate the intended hand motion of an operator. This network approximates a probability density function of discriminating data by a Gaussian mixture model through learning with sample data and can calculate *a posteriori* probability of the operator's motion with high discrimination performance from EMG patterns. Accordingly, the proposed system can be manipulated by an operator who does not have knowledge of EMG signals.

The input of the LLGMN $\mathbf{X}(n) \in \Re^H$ is calculated with the vector $\mathbf{x}(n) \in \Re^L$ as follows:

$$\mathbf{X}(n)=[1,\mathbf{x}(n)^{\mathrm{T}},x_1(n)^2,x_1(n)x_2(n),\cdots,x_1(n)x_L(n),\\ x_2(n)^2,x_2(n)x_3(n),\cdots,x_2(n)x_L(n),\cdots,x_L(n)^2]^{\mathrm{T}} \tag{3}$$

The first layer consists of $H(=1+L(L+3)/2)$ units corresponding to the dimension of $\mathbf{X}(n)$, and the identity function is used for an activation function of each unit. The output of the unit h, ${}^{(1)}O_h(n)$, is the same value of ${}^{(1)}I_h(n)$:

$${}^{(1)}I_h(n)=\mathbf{X}_h(n), \tag{4}$$

$${}^{(1)}O_h(n)={}^{(1)}I_h(n). \tag{5}$$

The second layer consists of the same number of units as the total number of components of the Gaussian mixture network. Each unit of the second layer receives the output of the first layer ${}^{(1)}O_h(n)$ weighted by the coefficient $w_h^{(k,m)}$, and outputs *a posteriori* probability of each component. The relationship between the input ${}^{(2)}I_{k,m}(n)$ and the output ${}^{(2)}O_{k,m}(n)$ in the second layer is defined as

$${}^{(2)}I_{k,m}(n)=\sum_{h=1}^{H}{}^{(1)}O_h(n)w_h^{(k,m)}, \tag{6}$$

$${}^{(2)}O_{k,m}(n)=\frac{\exp[{}^{(2)}I_{k,m}(n)]}{\sum_{k'=1}^{K}\sum_{m'=1}^{M_{k'}}\exp[{}^{(2)}I_{k',m'}(n)]}, \tag{7}$$

where $w_h^{(K,M_K)}=0$ $(h=1,2,\cdots,H)$. Note that (7) can be considered a generalized sigmoid function (Tsuji et al., 1994).

The unit k in the third layer integrates the outputs of M_k units in the second layer, and the relationship between the input ${}^{(3)}I_k(n)$ and the output ${}^{(3)}O_k(n)$ is described as

$${}^{(3)}I_k(n)=\sum_{m=1}^{M_k}{}^{(2)}O_{k,m}(n), \tag{8}$$

Table 1. Structure of the LLGMN (Fukuda et al., 2003)

The 1st layer	Number of units	H
	Input	$\mathbf{X}_h(n)$
	Output	$^{(1)}O_h(n)$
	I/O function	Identity function
The 2nd layer	Number of units	$\sum_{k=1}^{K} M_k$
	Input	$^{(2)}I_{k,m}(n)=\sum_{h=1}^{H(1)} O_h(n)w_{k,m,h}^{(2)}$
	Output	$^{(2)}O_{k,m}(n)$
	I/O function	Generalized sigmoid function
The 3rd layer	Number of units	K
	Input	$^{(3)}I_k(n)=\sum_{m=1}^{M_k(2)} O_{k,m}(n)$
	Output	$^{(3)}O_k(n)$
	I/O function	Identity function
Weight coefficients from 1st layer to 2nd layer		$w_{k,m,h}^{(2)}$
Weight coefficients from 2nd layer to 3rd layer		1

$$Y_k(n)={}^{(3)}I_k(n). \tag{9}$$

The output of the third layer $Y_k(n)$ corresponds to *a posteriori* probabilities of the class k for the inputted EMG pattern $\mathbf{x}(n)$. The detailed structure of the LLGMN is presented in Table 1.

Next, the network's learning method is explained. Consider a supervised learning with a teacher vector $\mathbf{T}^{(n)}=[T_1^{(n)},\cdots,T_k^{(n)},\cdots,T_K^{(n)}]^{\mathrm{T}}$ for the nth input vector $\mathbf{x}(n)$. If a teacher provides a perfect classification, $T_k^{(n)}=1$ for the particular class k and $T_k^{(n)}=0$ for all other classes. LLGMN is trained using a given set of N data $\mathbf{x}(n)$ $(n=1,2,\cdots,N)$ to maximize the likelihood function. The employed energy function J for the network training is defined as

$$J=\sum_{n=1}^{N} J_n=-\sum_{n=1}^{N}\sum_{k=1}^{K} T_k^{(n)} Y^k(n), \tag{10}$$

and the learning is performed to minimize this energy function (i.e., to maximize the likelihood function). The learning rule is designed with the concept of terminal attractor (TA) so that the convergence time of the function can be specified (Fukuda et al., 2003; Tsuji et al., 1994).

The proposed system uses off-line learning in the preliminary stage to perceive the EMG patterns corresponding to each of Kth target motions, while the online learning method adapts for the variation of EMG properties caused by muscle fatigue, sweat, and so on.

Task Estimation Using Petri Nets

In operating a dual-arm system, the operator has to skillfully coordinate the motions of right and left robotic arms. However, the classification results from the EMG pattern cannot be adopted directly because they are not considered to other arm conditions. This part estimates a task state of the coordinated tasks by the dual arms based on the time history of task states.

Let us imagine that an operator is pouring water into a cup held by the left arm from a bottle held by the right arm. In this task, a human should not drop a glass or bottle from their hand while pouring water. In this study, such a task flow is described with a task model using Petri nets (Reisig, 1988) that are proper for dealing with an event-driven task. Thus, the proposed system can estimate current task states and can regulate control parameters according to the estimated task states.

A task model $N=(P,T;F,M)$ can be expressed with the place set $P=\{p_0,p_1,\cdots,p_p\}$, the transition set $T=\{t_0,t_1,\cdots,t_T\}$, the arc set $F\subseteq(P\times T)\cup(T\times \Pi)$, and the initial marking set $M: P\rightarrow \mathbf{N}\cup\{\omega\}$. $\mathbf{N}$ indicates a set of positive integers, and ω is the infinity. T and P denote the numbers of transitions and places. The initial marking $m_0\in M$ is settled on the place p_0 that corresponds to the standby state (Fukuda et al., 2002).

Figure 3 presents an example of the task model using Petri nets, where a token denotes the current state (the standby state), and the branch subnets connecting this place represent the details of each task. The tree structure of the task model is suitable for recomposing its structure according to the change of tasks.

The task model calculates a modifying vector γ_m according to the estimated task state by

$$\gamma_m=[\gamma_{m0},\gamma_{m1},\cdots,\gamma_{mK},\gamma_{m(K+1)}]^T \tag{11}$$

where $m\in\{0,1,2,\cdots,P\}$ is the index of the place in the task model; $\gamma_{m1},\cdots,\gamma_{mK}$ indicates the weights corresponding to the motions; γ_{m0} and $\gamma_{m(K+1)}$ the modifying weights of a do-nothing operation and a suspending motion, respectively.

The modifying vector is then sent to the motion determination part. Also, the estimated power $F_{EMG}(n)$ given in (2) is modified using the parameters f_m as

$$F_{EMG}(n)=\frac{1}{L}\sum_{i=1}^{L}\frac{EMG_i(n)-\overline{EMG_i}^{st}}{EMG_i^{max}-\overline{EMG_i}^{st}}f_m. \tag{12}$$

Motion Determination

Motion is determined by the estimated force $F_{EMG}(n)$ given in (12), and the probability of the do-nothing operation $Y_0(n)$ is calculated by the following membership function:

$$Y_0(n) = -\frac{1}{\pi}\tan^{-1}\{A_1(F_{EMG}(n) - B_1)\} + 0.5, \tag{13}$$

where A_1 and B_1 are positive constants. The value of $Y_0(n)$ approaches 1 as $F_{EMG}(n)$ approaches 0, while $Y_0(n)$ decreases as $F_{EMG}(n)$ increases as presented in Figure 4(a).

Next, to evaluate the accuracy of discrimination results by the neural network, the probabilities of suspending motion $Y_k(n)$ ($k = 1,2,\cdots,K$: K is the number of target motions) is defined with the entropy $H(n)$:

$$H(n) = -\sum_{k=1}^{K} Y_k(n)\log Y_k(n). \tag{14}$$

The entropy is calculated by *a posteriori* probabilities of the operator's motions that are the output of the trained LLGMN, which may be interpreted as a risk of ill recognition. For example, the entropy is low when the energy function is thoroughly reduced, in which one of *a posteriori* probabilities takes a remarkably large value and the other ones are close to 0. In contrast, when the output of LLGMN is ambiguous, the entropy is high. This entropy tends to increase when EMG patterns are disturbed by an unexpected external event, such as the switching of the operator's motions and unexpected noise signals.

Figure 3. An example of the task model

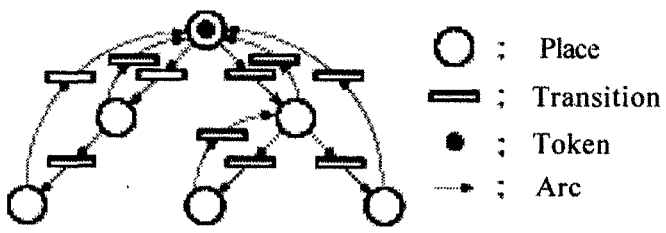

By means of the entropy given by (14), the probability of suspending motion $Y_{K+1}(n)$ is defined as

$$Y_{K+1}(n) = \frac{1}{\pi}\tan^{-1}\{A_2(H(n) - B_2)\} + 0.5, \tag{15}$$

where A_2 and B_2 are positive constants. If the entropy $H(n)$ is close to 0, $Y_{K+1}(n)$ becomes close to 0. However, if $H(n)$ increases, $Y_{K+1}(n)$ is close to 1 as indicated in Figure 4(b).

Finally, the motion k with the maximum value of the probability $O_k(n)$ is selected as the operator's intended motion:

$$O_k(n) = \frac{\gamma_{mk} Z_k(n)}{\sum_{j=1}^{K+1} \gamma_{mj} Z_j(n)}, \tag{16}$$

where $Z_k(n)$ $(k = 0,1,\cdots,K,K+1)$ is calculated using $Y_0(n)$, $Y_{K+1}(n)$, and $Y_k(n)$ $k = 0,1,\cdots,K)$ as

$$Z_k(n) = \begin{cases} Y_k(n) & (k=0) \\ (1-Y_0(n))(1-Y_{K+1}(n))Y_k(n) & (k=1,2,\cdots,K), \\ (1-Y_0(n))Y_k(n) & (k=K+1) \end{cases} \tag{17}$$

Adaptive Learning Algorithm

When the operator controls the dual-arm manipulator for many hours, it is necessary to consider variations of EMG properties resulting from muscle fatigue, sweat, and the change of the characteristics and the electrode position. The muscles of a non-dominant arm fatigue more readily compared to the dominant arm. Therefore, an online learning method that can adapt to such variations of EMG properties is needed to discriminate the EMG pattern successively for a long-term operation. However, the correct teacher signals cannot be obtained in the operation since it is impossible to directly find the operator's intended motion.

Figure 4. Membership functions for do-nothing operation and suspending motion ($A_1 = 4.0$, $B_1 = 0.5$, $A_2 = 8.0$, $B_2 = 0.7$)

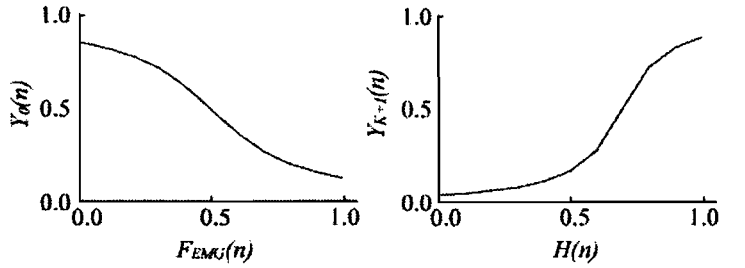

(a) Possibility of no motion (b) Possibility of suspending motion

For that, the replacement of learning data and the relearning of LLGMN are executed according to the reliability of outputs of the LLGMN for the EMG pattern $\mathbf{x}(n)$, that is, the entropy $H(n)$ given in (14). If the entropy $H(n)$ is less than a given threshold H_0, the EMG pattern $\mathbf{x}(n)$ is replaced with the oldest pattern in the set of the stored learning data. The weights of LLGMN are then updated using the new set of the learning data only when the energy function J is decreased by the relearning procedure to avoid incorrect learning.

Bio-Mimetic Impedance Control

Generally speaking, a human forearm is compliant when holding a soft object, while it stiffens when holding a hard or heavy one. Such dynamic properties of human movements can be represented by the mechanical impedance parameters: stiffness, viscosity, and inertia (Tsuji et al., 1995). If the human impedance characteristics of the forearm can be applied to control the robotic manipulator, it is possible to realize natural movements like a human forearm. This system tries to realize natural motions of the end-effectors by using the human impedance characteristics estimated from EMG signals (Fukuda et al., 2002).

The dynamic equation of the jth joint of the prosthetic forearm under impedance control is defined as

$$I_j\ddot{\theta}_j + B_j(\alpha_j)\dot{\theta}_j + K_j(\alpha_j)(\theta_j - \theta_j^e) = \tau_j^{ex}, \tag{18}$$

$$\theta_j^e = \frac{\alpha_j \tau_{jk}^{max}}{K_j(\alpha_j)}, \tag{19}$$

where I_j, $B_j(\alpha_j)$, and $K_j(\alpha_j)$ are the inertia, viscosity, and stiffness. The viscosity and the stiffness are related to the muscular contraction ratio α_j represented by a non-linear model using α_j (Fukuda et al., 2002). θ_j and θ_j^e are the measured and equilibrium angles of the jth joint, and τ_j^{ex} and τ_{jk}^{max} are the external torque and the prespecified maximal torque for the motion k.

The driven joint j is selected according to determination result k in the motion determination part. The muscular contraction ratio α_j is defined using $F_{EMG}(n)$ as

$$\alpha_j(n) = \frac{F_{EMG}(n)}{EMG_k^{max}}, \tag{20}$$

where EMG_k^{max} is the mean value of F_{EMG} while keeping the maximum voluntary contraction (MVC) for motion k (k = 1,2,···,K). If a discriminated motion is determined as the suspending motion, the motion keeps the last motion as $\tau_j(n) = \tau_j(n-1)$.

The desired joint angles are calculated in the impedance filter part, and they are controlled using the tracking control part as illustrated in Figure 5, where K_p, K_i, K_v are the gain parameters for a PID control method. This method realizes a natural feeling of control similar to that of the original limb, if the impedance parameters are set to similar values of the human arm. In this system, the impedance parameters are updated to suitable values according to the task state estimated by a task model.

Upper Arm Control Part

The upper arm control part uses a 3-D position sensor (ISOTRACK II: POLHEMUS, Inc.) as an input device for the control signal. The operator

Figure 5. Block diagram of a biomimetic impedance control part

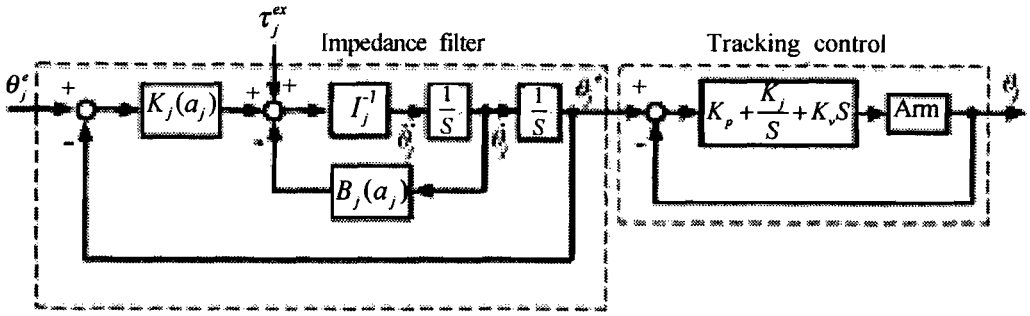

attaches this sensor at his or her wrist, and the desired joint angles of the forearm ($\theta_{1w}, \theta_{2w}, \theta_{3w}$) are calculated from the measured operator's wrist position. The motion of each joint is controlled by the PID control method. The system adopts the non-contact impedance control (Tsuji & Kaneko, 1999) to adjust dynamic characteristics of the dual-arm according to the relative movements between them.

Figure 6 schematically represents the non-contact impedance control. Consider the case in which an object (the left end-effector) approaches the right manipulator, and set a virtual sphere with radius r at the center of the end-effector. When the object enters the virtual sphere, the normal vector from the surface of the sphere to the object $dX_0 \in \Re^l$ can be represented as

$$dX_o = X_r - rn, \tag{21}$$

$$n = \begin{cases} \dfrac{X_r}{|X_r|} & (X_r \neq 0) \\ 0 & (X_r = 0) \end{cases}. \tag{22}$$

When the object is in the virtual sphere ($|X_r| < r$), the virtual impedance works between the end-effector and the object so that the virtual external force $F_0 \in \Re^l$ is exerted on the end-effector by

$$F_o = \begin{cases} M_o d\ddot{X}_o + B_o d\dot{X}_o + K_o dX_o & (|X_r| \leq r) \\ 0 & (|X_r| > r) \end{cases}, \tag{23}$$

where M_o, B_o, and $K_o \in \Re^{l \times l}$ represent the virtual inertia, viscosity, and stiffness matrices. Note that $F_o = 0$ when the object is outside the virtual sphere or at the center of the sphere. Thus, the dynamic equation of the end-effector for non-contact impedance control can be expressed with (22) and (23) as

$$M_e d\ddot{X} + B_e d\dot{X} + K_e dX = F_{int} + F_0. \tag{24}$$

Because of the virtual sphere defined at the end-effector, a virtual external force F_0 is exerted on an end-effector of the manipulators, so that the robot can be

Figure 6. Schematic representation of a non-contact impedance control. One arm has virtual sphere, while the other arm does not have it.

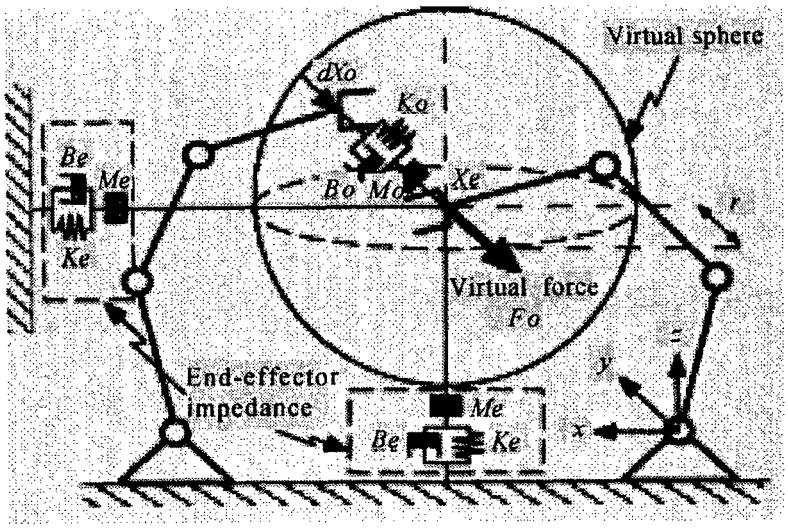

controlled before contact with the environment. Also, the existence and radius of the virtual spheres and virtual impedance parameters can be suitably changed by a task model during tasks.

Feedback Part

Before the operation is started, an operator has to check whether the EMG signals are measured by using the graphical feedback display, shown in Figure 7(a). After calculating $\overline{EMG_i}^{st}$ and EMG_i^{max} (Figure 7(b)), the EMG pattern is extracted for each motion to collect teacher vectors (Figure 7 (c)). The LLGMN is then trained with the teacher vectors (Figure 7(d)). Finally, the operator checks the motion-discriminated results (Figure 7(e)). If the discrimination results are improper, the teacher vectors are measured again for the learning of LLGMN.

The operator controls two manipulators by watching a set of monitors placed in front of him or her. The image sequence is captured by a pair of cameras as shown in Figure 8(a), and the computer graphics of the task environment are provided as feedback to the operator in Figure 8(b). Camera A is set up at the back of the manipulators, and Camera B is set up at the side of the right arm. Camera B uses Nu-View (3D.com, Inc.) to construct a 3-D perspective image, so that the operator can find three-dimensional information of the virtual environment by wearing LCD shutter glasses.

Figure 7. Graphical display for the myoelectric teleoperation

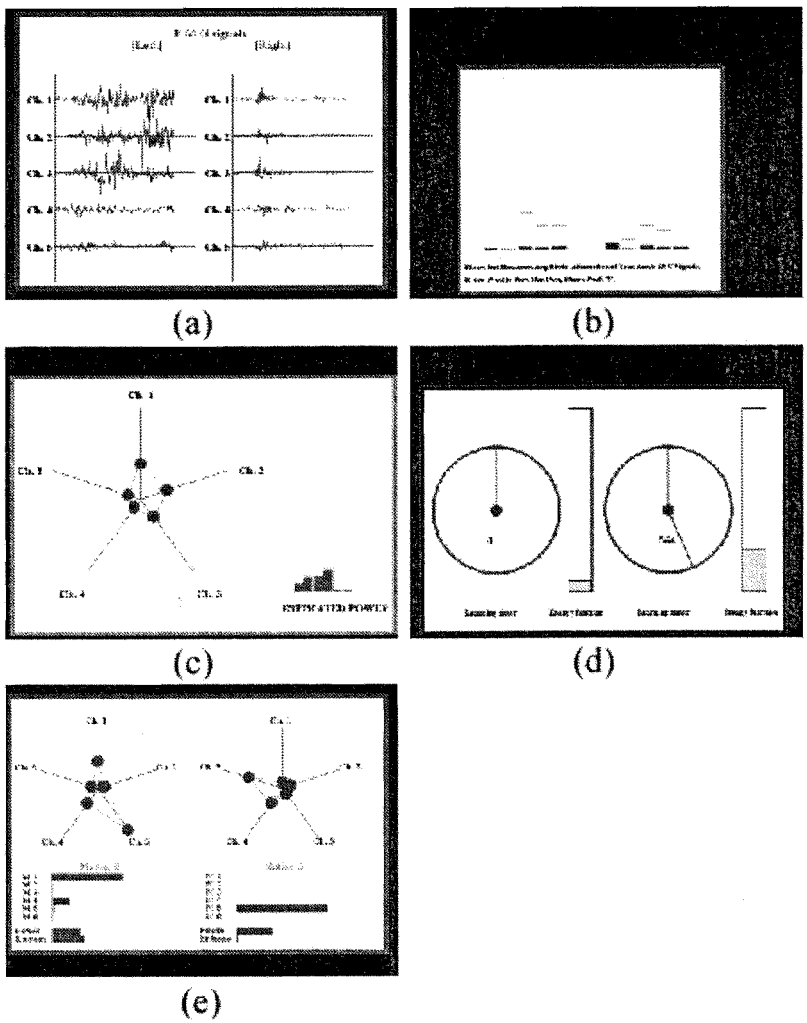

Figure 8. An operator maneuvering the teleoperation system via feedback displays

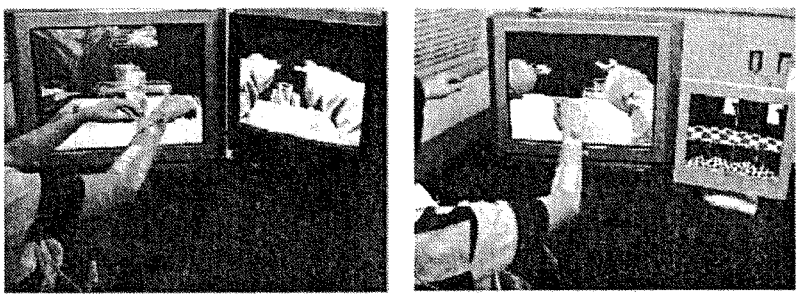

Figure 9. Experimental apparatus of the task environment in the remote place

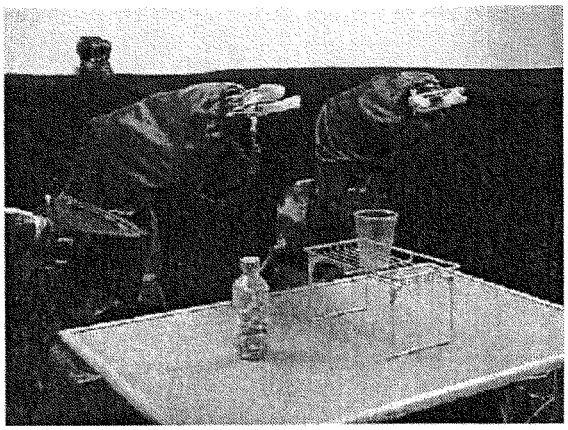

Experiments

Experiments were conducted with four male subjects (graduate students, 23-25 years old; Subjects A, B, and C: right handers; Subject D: left hander) to demonstrate the verification of the developed dual-arm manipulator system.

Operation of Dual-Arm Manipulator

A subject was asked to perform a given task including subtasks: grasp a bottle with the right hand, remove the bottle cap with the left hand, and pour from the bottle into a cup. Figure 9 shows the robot manipulators and task environment established in the remote place. Table 2 represents the eight task states and the eight primitive motions of the dual-arm manipulator prepared for the given task, while Figure 10 shows the designed task model using Petri nets in this chapter.

In the experiment, three pairs of electrodes (ch.1, 2, 3) were set at muscles of the operator's forearm, and two pairs of electrodes at muscles of the operator's upper arm (ch. 4, 5). Six motions are discriminated as a primitive hand motion (hand opening, hand closing, hand closing and pronation, hand opening and pronation, pronation, and supination). The control parameters in (13) and (15) were set as $(A_1,A_2,B_1,B_2) = (4.0, 4.0, 0.2, 0.3)$ for the right manipulator and (4.0, 4.0, 0.15, 0.3) for the left manipulator.

Figure 11 shows a typical scene of teleoperation of the dual-arm system for the given cooperation task by subject A. In each task state, a left photo gives operator's motion while a right one shows the dual-arm robot's motion teleoperated

Table 2. Places and transitions

(a) Places

p_0	Standby	p_3	Grasping a tube
p_1	Grasping a bottle	p_4	Grasping a tube and cup
p_2	Opening the cap	p_7	Pouring into a cup
p_3	Grasping a bottle and cup	p_8	Grasping a cup
p_4	Pouring into a cup		

(b) Transitions

t_0	Open	t_3	Grasp (left hand)
t_1	Grasp (right hand)	t_4	Grasp (right hand)
t_2	Grasp (left hand)	t_7	Pronation and Grasp (left hand)
t_3	Grasp (left hand)	t_8	Open (right hand)
t_4	Pronation (right hand)		

Figure 10. Task model used in experiments

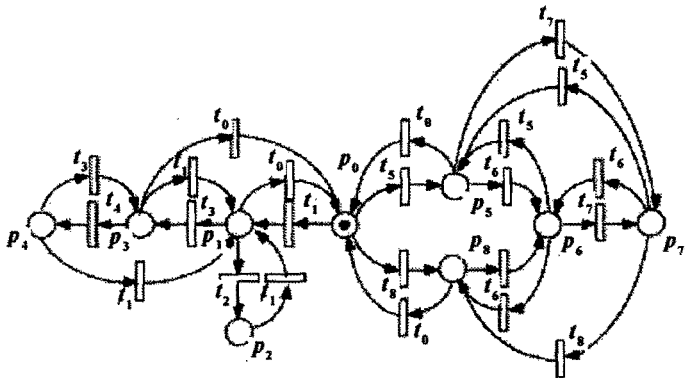

by the subject. Figure 12 represents time profiles of the EMG signals measured from the right and left arms, the estimated forces and discriminated motions of the right and left arms, and the estimated task states using Petri nets, in order from the top, during the operation shown in Figure 11. Since the motion discrimination is performed well, it can be seen that the subject can operate the proposed system properly by remote control using EMG signals to achieve the given task.

Motion-Discrimination with Adaptive Learning

The effectiveness of adaptive learning of neural networks for motion discrimination was examined using long-term (5-day) experiments. Subjects were asked to perform the same six motions as the ones in the previous subsection at regular intervals for 120 minutes; they executed almost 1,440 motions in this experiment.

Figure 11. An example of the dual-arm control

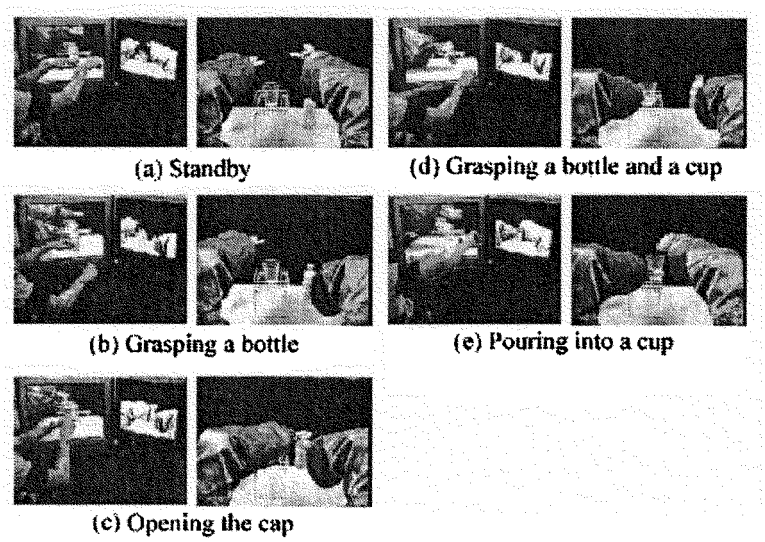

Figure 12. An example of the experimental results by subject A

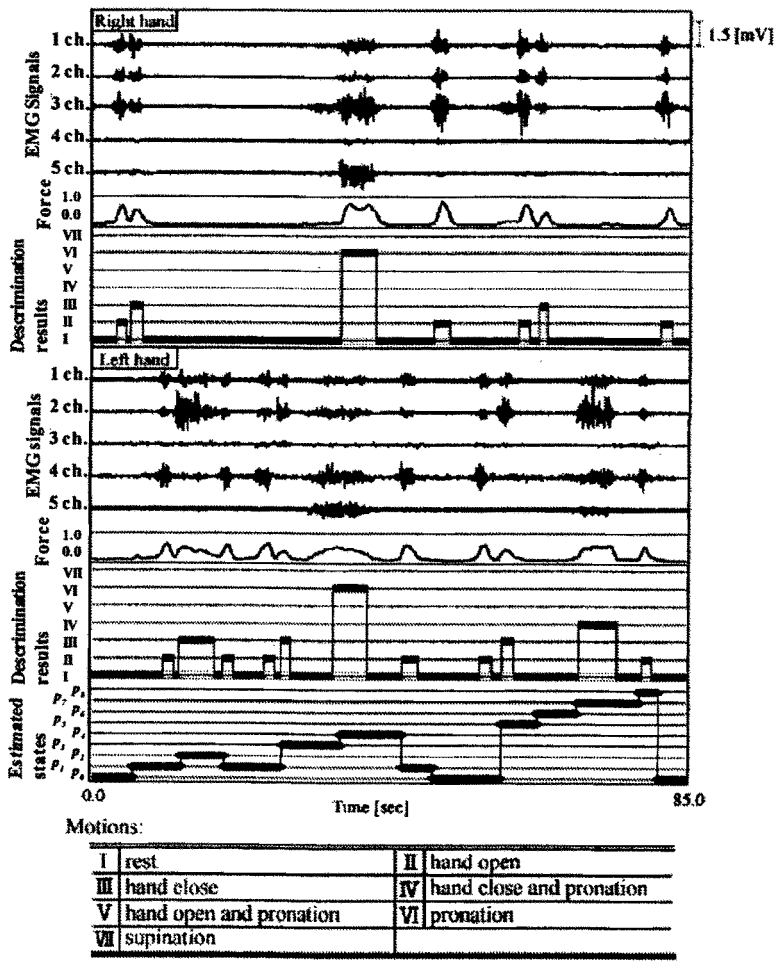

Figure 13. Effect of adaptive learning on the motion discrimination ability by subject A who is right-handed

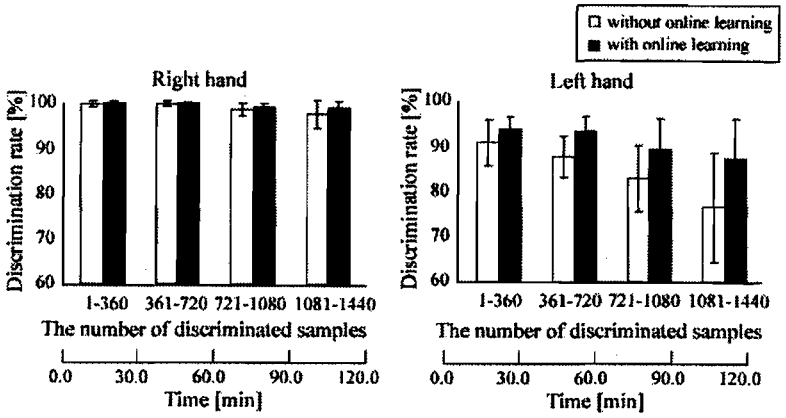

Figure 14. Experimental results of hand motion discrimination for four subjects

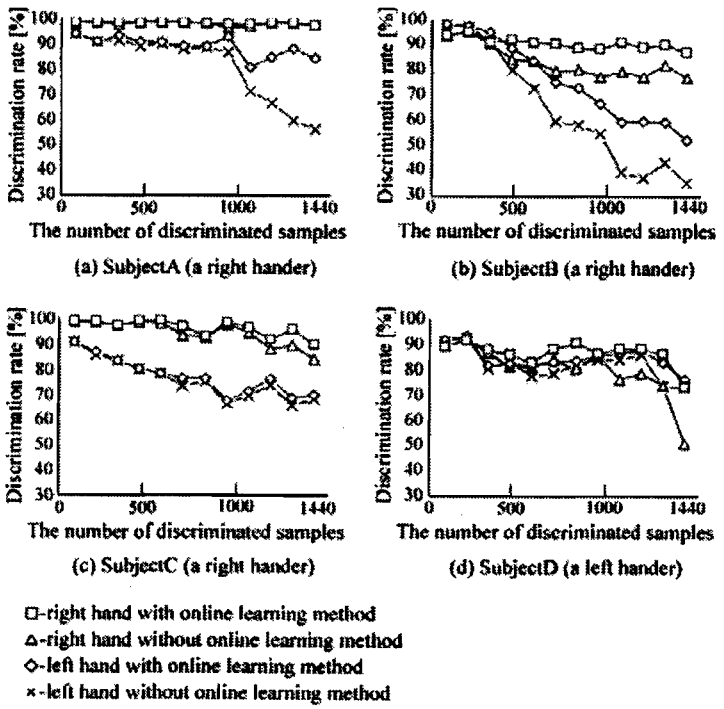

The adaptive learning of neural networks was carried out by setting the number of learning data at $N = 120$ and the learning thresholds H_o at 0.2. The subjects were not informed of the discrimination result to exclude intentional changes of EMG patterns during the experiment. Also, each element of the modifying vector $(\gamma_{m0},\cdots,\gamma_{m9K=1})$was set at 1.0.

Figure 13 shows the averages and standard deviations of discrimination rates by subject A, in which the discrimination rates were calculated every 360 motions. The discrimination rate without the online learning method decreased with time

because of the variation of EMG patterns caused by fatigue and/or sweat. It should be noted that the effectiveness of the online learning method can be observed clearly from the discrimination rates of the non-dominant hand.

Figure 14 presents the discrimination rates of all subjects calculated every 120 motions for one day. The discrimination rates of all subjects are high at the beginning of the experiment and tended to decrease as the operation continued. However, it can be seen that the rates are maintained at a sufficiently high level by using the online learning method.

Conclusion

This chapter has described a novel teleoperation technique using neural networks for a dual-arm manipulator system teleoperated by EMG signals. In the developed system, an operator is not physically constrained by a control device like the traditional master arm, so that he or she can control the manipulators by using bioelectric signals as hoped. The system utilizes an event-driven task model and non-contact impedance control to achieve skilled movements such as coordinated tasks by dual arms, and high discrimination performance can be attained by adapting the variation of EMG signals caused by individual differences, electrode locations, physical fatigue, sweat, and operator's posture.

The experimental results demonstrated that coordinated tasks can be performed with the proposed cybernetic control of the dual-arm system and that the high accuracy of motion discrimination can be maintained by the proposed adaptive learning method of neural networks even after the operator has controlled the manipulators for a long period of time.

The teleoperation system using EMG signals has enough potential as an operational interface to maneuver robotic manipulators by remote control intuitively. In future research, we would like to establish a task model with learning ability and feedback enhancement. We also plan to expand the developed dual-arm manipulator using EMG signals into a human-assisting system for the handicapped, such as an amputee and the aged (Fukuda et al., 2003).

Acknowledgments

The authors would like to thank Dr. O. Fukuda of National Institute of Advanced Industrial Science and Technology (AIST). This research work was supported in part by a Grant-in-Aid for Scientific Research from the Japanese Ministry of

Education, Science and Culture (11555113, 15360226, and 16760203). The support from New Energy and Industrial Technology Development Organization (NEDO) of Japan is also much appreciated.

References

Englehart, K., & Hudgins, B. (2003, July). A robust, real-time control scheme for multifunction myoelectric control. *IEEE Transactions on Biomedical Engineering, 50*(7), 848-854.

Farry, K. A., Walker, I. D., & Baraniuk, R. G. (1996). Myoelectric teleoperation of a complex robotic hand. *IEEE Transactions on Robotics and Automation, 12*(5), 775-788.

Fukuda, O., Tsuji, T., Kaneko, M., & Otsuka, A. (2003, April). A human-assisting manipulator teleoperated by EMG signals and arm motions. *IEEE Transactions on Robotics and Automation, 19*(2), 210-222.

Fukuda, O., Tsuji, T., Takahashi, K., & Kaneko, M. (2002). Skill assistance for myoelectric control using an event-driven task model. *Proceedings of the 2002 IEEE/RSJ International Conference on Intelligent Robots and Systems (IROS2002),* 1445-1450.

Goertz, R. C. (1954). Manipulator systems development at ANL. *Proceedings of the 12th Conference on Remote Systems Technology* (pp. 117-136). American Nuclear Society.

Kim, K. -Y., Kim, D. -H., Jeong, Y., Kim, K., & Park, J. -O. (2001). A biological man-machine interface for teleoperation. *Proceedings of the 32nd International Symposium on Robotics,* 574-579.

Mobasser, F., Hashtrudi-Zaadand, K., & Salcudean, S. E. (2003). Impedance reflecting rate mode teleoperation. *Proceedings of the 2003 IEEE International Conference on Robotics and Automation (ICRA2003),* 3296-3302.

Reisig, W. (1988). *Petri nets.* Springer-Verlag.

Sheridan, T.B. (1992). *Telerobotics, automation and human supervisory control.* MIT Press.

Shimamoto, M.S. (1992). Teleoperator/telepresence system (TOPS) concept verification model (CVM) development. *Recent Advances in Marine Science and Technology,* 97-104.

Suryanarayanan, S., & Reddy, N.P. (1997). EMG based interface for position tracking and control in VR environments and teleoperation. *Teleoperators and Virtual Environments, 6*(3), 282-291.

Tsuji, T., Fukuda, O., Ichinobe, H., & Kaneko, M. (1999, February). A log-linearized Gaussian mixture network and its application to EEG pattern classification. *IEEE Transactions on System, Man and Cybernetics, Part C, Applications and Reviews, 29*(1), 60-72.

Tsuji, T., Ishinobe, H., & Makoto, M. (1994). A proposal of the feedforward neural network based on the Gaussian mixture model and the log-linear model (in Japanese). *The Transactions of the Institute of Electronics, Information and Communication Engineers, J77-D-II*(10), 2093-2100.

Tsuji, T., & Kaneko, M. (1999). Non-contact impedance control for redundant manipulators. *IEEE Transactions on Systems, Man, and Cybernetics, Part A, Systems and Humans, 29*(2), 184-193.

Tsuji, T., Morasso, P. G., Goto, K., & Ito, K. (1995). Human hand impedance characteristics during maintained posture. *Biological Cybernetics, 72*, 457-485.

Tsujiuchi, N., Koizumi, T., & Yoneda, M. (2004). Manipulation of a robot by EMG signals using linear multiple regression model. *Proceedings of the 2004 IEEE/RSJ International Conference on Intelligent Robots and Systems (IROS2004),* 1991-1996.

Ueda, J., & Yoshikawa, T. (2004, June). Force-reflecting bilateral teleoperation with time delay by signal filtering. *IEEE Transactions on Robotics and Automation, 20*(3), 613-619.

Wolpaw, J. R., Ramoser, H., McFarland, D. J., & Pfurtscheller, G. (1998). EEG-based communication: Improved accuracy by response verification. *IEEE Transactions on Rehabilitation Engineering, 6*, 326-333.

Yokokohji, Y., & Yoshikawa, T. (1994). Bilateral control of master-slave manipulators for ideal kinesthetic coupling. *IEEE Transactions on Robotics and Automation, 10*, 605-620.

Yoon, W.-K., Goshozono, T., Kawabe, H., Kinami, M., Tsumaki, Y., Uchiyama, M., Oda, M., & Doi, T. (2001). Model-based teleoperation of a space robot on ETS-VII using a Haptic Interface. *Proceedings of the 2001 IEEE International Conference on Robotics and Automation (ICRA2001),* 407-412.